

ADDITIVE MANUFACTURING OF NOVEL HIGH STRENGTH ALUMINIUM ALLOYS

M.L. Montero-Sistiaga[1], M. de Smit[1], A. Pastor Muro[2], N. Redondo Torrico[2], M. Thomas[3], A. Morel[3], S. Drawin[3], and F. Palm[4]

[1]Royal NLR-Netherlands Aerospace Centre, 8316 PR Marknesse, The Netherlands.

[2]National Institute of Aerospace Technology (INTA), 28850 Torrejón de Ardoz, Spain

[3]DMAS, ONERA, Paris Saclay University, 92320 Châtillon, France

[4]Airbus, Central Research & Technology (CRT), 82024 Taufkirchen, Germany

Abstract

This study investigates the additive manufacturing of novel high-strength aluminium alloys using laser powder bed fusion (L-PBF). Two alloy systems, Scancromal® and Lean-Scancromal®, were characterised and processed to evaluate their suitability for aerospace applications. The study was divided in two routes: extensive powder characterisation and optimisation the processability by L-PBF process. Powder characterisation revealed spherical particles with limited satellite formation, suitable for L-PBF processing. Process parameter optimisation was carried out using thin walls and variable hatch blocks to identify suitable laser parameter combinations for both alloys. The results demonstrated promising L-PBF processability for both alloy systems, with Lean-Scancromal showing a narrower particle size distribution and Scancromal exhibiting slightly better flowability behaviour. The study contributes to the wider industrial implementation of high-strength aluminium alloys for aerospace additive manufacturing applications.

Keywords: Additive Manufacturing, High strength aluminium alloys, Process optimisation,

Microstructure, Mechanical testing

1. General Introduction

Aluminium and its alloys are widely used in the aerospace sector due to their excellent mechanical performance in combination with their light weight. Their strength and low density are the main advantages of these materials. Fabricating components with complex geometries from high strength aluminium alloys by conventional processing techniques is challenging due to their low formability. In contrast, metal Additive Manufacturing (AM) techniques allow the production of near-net-shape and complex parts, adding value to the use of aluminium alloys in the aerospace sector [1], [2]. Even so, not all aluminium alloys are easy to process by AM [3].

Currently, there are several novel aluminium alloys being investigated for application in AM. Significant progress has been reported on laser powder bed fusion (L-PBF) [4], [5] and directed energy deposition (DED) [6]. One of the main research focuses is to broaden the materials palette towards higher-performance aluminium alloys. On one hand, the high-strength 7000 series has been investigated aiming at avoiding solidification cracking during the AM process. Several works have focused on modifying the composition by additions of Zr [4], Sc [7] or Si [5] in order to avoid cracking and improve the mechanical properties. On the other hand, casting aluminium alloys have been

widely investigated with the addition of nano-/micron-sized particles such as TiB_2 [8] or TiC [9] aiming at increased fatigue performance. Examples of these modifications have resulted in commercially available aluminium alloys such as A20X™ [10] developed by Aeromet with Cu and TiB_2, or Scalmalloy® [11] developed by Airbus & commercialised by APWorks.

The investigated alloy systems were selected due to their potential to achieve crack-free processing combined with high mechanical performance in AM conditions.

Besides the advancements on alloy development for AM, there is still a big gap with respect to commercialisation of these novel alloys. In addition, aluminium alloys are particularly challenging for laser-based additive manufacturing due to their high laser reflectivity, elevated thermal conductivity and susceptibility to solidification cracking and gas porosity. Therefore, significant efforts are still required to fully characterise these compositions in order to obtain a comprehensive overview of their mechanical performance under different processing conditions.

In this work, two novel aluminium alloy powders, Scancromal® and Lean-Scancromal®, were characterised and processed by laser powder bed fusion (L-PBF). Powder characterisation and L-PBF processability were evaluated prior to process parameter optimisation. Thin wall and variable hatch block strategies were employed to identify optimum processing parameters aimed at minimising porosity and improving process stability. The optimisation of these alloy systems is expected to contribute to the wider industrial implementation of high-strength aluminium alloys in aerospace additive manufacturing applications.

2. Materials and methods

2.1 Powder characterisation

The powders were manufactured by Toyo Aluminium KK (TOYAL), Hino, Japan. Different powder batches of Scancromal® and Lean-Scancromal® alloys were received and analysed in order to evaluate powder consistency and L-PBF processability.

The particle size distribution (PSD) was measured by sieve analysis, laser diffraction and scanning electron microscope (SEM) image analysis in order to compare the three techniques. Sieve analysis was performed at INTA facilities using a FRITSCH model 3502, laser diffraction was performed in ONERA using a HORIBA LA-950V2 analyser and finally, scanning electron microscope (SEM) image analysis using a FEI Nova NanoSEM .

Powder chemical composition was analysed by inductively coupled plasma optical emission spectroscopy (ICP-OES) using a Metrohm SpectroGreen spectrometer. The technique was employed to determine the concentration of the main alloying elements and evaluate the agreement with the target alloy specifications.

Powder morphology analysis by SEM was carried out by ONERA.

The powder flowability was evaluated using a tapping device and Hall flow meter by NLR. The apparent and tapped densities were obtained using a GranuPack system according to ISO-4490, ASTM-B213 and MPIF-3 standards. From these measurements, Hausner ratio (HR), Carr index (CI), and characteristic tap number n1/2 at half compaction were obtained, which help classify powders in terms of flowability and processability. The Hall flow test was performed according to ISO 3923-1 standard. The average of three measurements was taken.

2.2 Process optimisation

The two received powders were processed in a SLM Solution 280HL machine equipped with a 400 W laser and in-house improved circulation gas system. For the process optimization, first thin walls were produced to allow the selection of parameters for the contours. The scan speed (*v*) was varied from 350 to 667 mm/s and the laser power (*P*) from 88 - 334 W. Next, blocks were produced with variable hatch spacing from 0.1 to 0.2 mm. Each block was manufactured using a specific combination of *P* and *v*. The scan speed was varied from 431 to 1520 mm/s and the laser power from 280 to 380 W.

The selection of the parameters was done by evaluating the optical microscopy images of the thin walls and blocks. For that, the samples were mounted and polished using diamond-based polishing solution. A Zeiss Axioplan 2 microscope was used for optical imaging. The thin walls were evaluated in terms of porosity, thickness and roughness. The variable hatch block were evaluated by analysing the porosity of the cross-sections.

3. Results and discussion

The powder characteristics and L-PBF processability of Scancromal® and Lean-Scancromal® powders were investigated through particle size distribution analysis, SEM morphology observations and flowability measurements. In addition, process parameter optimisation was carried out by evaluating thin walls and variable hatch blocks in terms of porosity, roughness and geometrical stability.

3.1 Powder characterization

3.1.1 L-PBF Particle size distribution

Particle size distribution (PSD) was evaluated by sieve analysis, SEM image analysis and laser diffraction in order to compare the different characterisation techniques and assess powder suitability for L-PBF processing.

PSD by sieve analysis was performed using sieves ranging from 20 to 90 µm. The sieve distribution results, summarised in Table 1, indicated PSD ranges compatible with L-PBF processing requirements. For L-PBF Lean-Scancromal powder, approximately 69% of the particles were within the 44–63 µm range, as shown in Table 1, which is suitable for stable powder spreading during L-PBF manufacturing.

Table 1 Sieve size distribution for L-PBF Scancromal powder.

	Percentage (%)	
Sieve size (µm)	**LPBF Scancromal**	**LPBF Lean Scancromal**
>90		0.04
75 - 90	0.11	0.18
63 - 75	18.11	0.87
56 - 63	45.27	39.66
44 - 56	26.05	29.27
37 - 44	8.63	18.00
20 - 37	0.05	8.03
0 - 20	1.79	3.98

PSD was also calculated based on both mean particle diameter and equivalent particle volume measured from SEM images.

The PSD values obtained from SEM analysis are summarised in Table 2. Lean-Scancromal exhibited a narrower particle size distribution and smaller mean particle diameter values compared to Scancromal powder.

Table 2 Calculated PSD values [µm] for Scancromal and Lean-Scancromal based on SEM images.

	L-PBF Scancromal		**L-PBF Lean-Scancromal**	
(µm)	Diameter	Volume	Diameter	Volume
D10	14.06	35.12	13.36	26.45
D50	36.80	52.48	27.08	42.15
D90	59.06	69.01	46.89	57.75

The measured PSD values obtained by laser diffraction, summarised in Tables 3 and 4, were found to be in good agreement with the supplier data for both alloy systems.

Granupack measurements additionally demonstrated suitable packing behaviour and flowability for L-PBF applications, with Hausner ratio and Carr index values characteristic of powders exhibiting good L-PBF processability.

Table 3 PSD values obtained by laser diffraction for L-PBF Lean-Scancromal powder

L-PBF Lean-Scancromal		
(µm)	Toyal data (supplier)	ONERA data
D10	25.6	26.5
D50	41.2	35.7
D90	62.4	49.4

Table 4 PSD values obtained by laser diffraction for L-PBF Scancromal powder

Scancromal		
(µm)	Toyal data (supplier)	ONERA data
D10	32.8	34.1
D50	48.0	49.0
D90	68.9	71.9

3.1.2 Chemical composition

The chemical composition of both powders, summarised in Table 5, was analysed by inductively coupled plasma optical emission spectroscopy (ICP-OES). The alloy systems were specifically designed to improve L-PBF processability while maintaining high mechanical performance. The obtained compositions were consistent with the targeted alloy design and suitable for further L-PBF parameter optimisation studies.

Table 5 Chemical composition of Scancromal and Lean-Scancromal powders as measured by INTA and Airbus.

Wt.%	**Scancromal**			**Lean-Scancromal**		
Element	Spec.	(AIRBUS)	(INTA)	Spec.	(AIRBUS)	(INTA)
Al	Bal	Bal	Bal	Bal	Bal	Bal
Cr	3 - 4	3.8	3.77	1.5 - 2	1.6	1.46
Mg		0.02	0.02	0.8 - 1.3	1.1	0.94
Sc	0.6 - 0.8	0.68	0.70	0.4 - 0.6	0.49	0.44
Mo	1 - 1.5	1.3	1.36	0.4 - 0.8	0.59	0.63
Zr	0.3 - 0.6	0.45	0.45	0.2 - 0.4	0.28	0.24
Si		0.09	0.084		0.13	0.08
Fe		0.24	0.27		0.10	0.12
Mn		<0.01	0.006		-	-
Ti		-	-		<0.01	<0.006
Ni		-	-		<.006	<0.006
Zn		-	-		-	<0.005
V		-	-		-	0.01
O		-	-		-	0.03
N		-	-		-	-

3.1.3 Flowability

Powder flowability was evaluated through Hall flow measurements and GranuPack analysis. Apparent and tapped densities were used to calculate Hausner ratio (HR) and Carr index (CI), which are commonly employed to assess powder flowability and processability.

The Hall flow and apparent density results are summarised in Table 6. Both powders exhibited suitable flowability for L-PBF processing, with stable packing behaviour and acceptable flow characteristics. Lean-Scancromal showed slightly higher Hall flow times, whereas similar apparent density values were obtained for both alloy systems.

These results are particularly important for achieving homogeneous powder deposition and stable layer-by-layer manufacturing during L-PBF processing.

Table 6 Hall flow and apparent density.

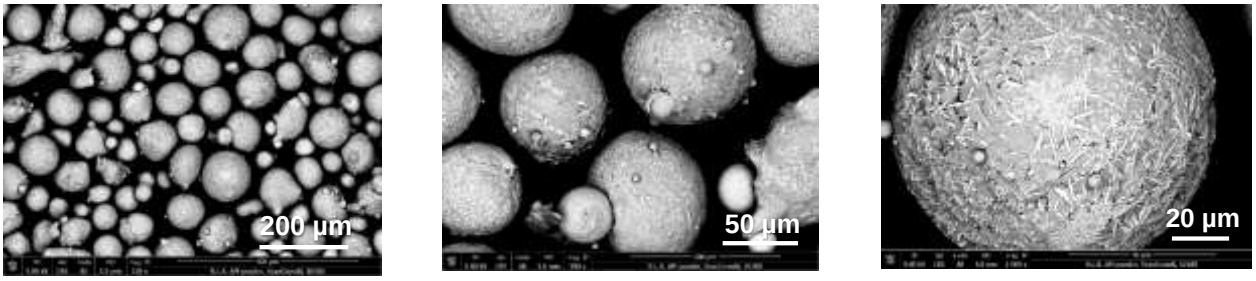
	L-PBF Scancromal	**L-PBF Lean-Scancromal**
Hall flow (s/50 g)	57.8 ± 3.5	67.3 ± 2.1
Apparent density (%)	53.0	54.0

3.1.4 Powder Morphology L-PBF

Two L-PBF powder batches were characterised: Scancromal and the Lean-Scancromal, the latter being designed with lower Cr and Sc contents.

Three types of observations were performed using SEM. The surface of the Scancromal particles has been examined for the evaluation of sphericity and surface roughness. Particles have also been polished to examine any internal defects. The internal microstructure of Scancromal and Lean-Scancromal particles has been observed using back-scattered electron (BSE) mode. Finally, Energy-dispersive X-ray spectroscopy (EDX) has been employed for semi-quantitative chemical analysis through the present phases.

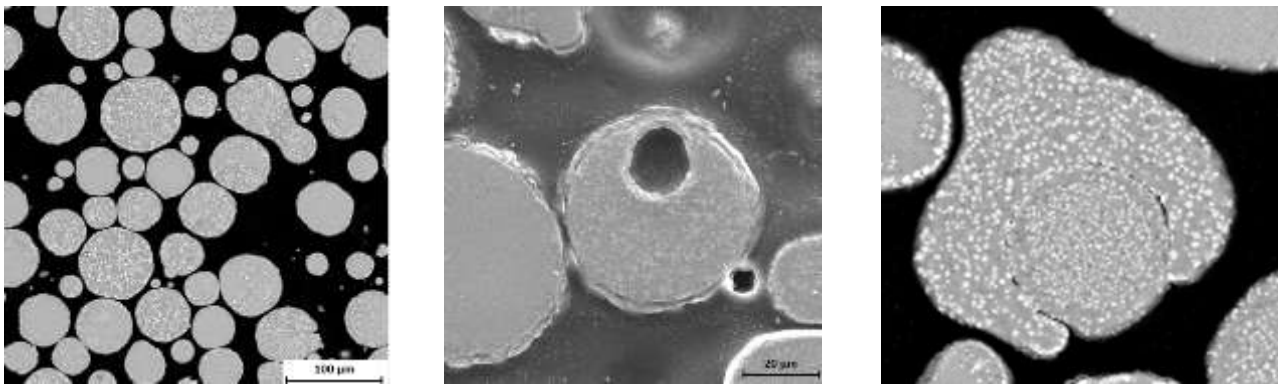
Micrographs showing the surface of the Scancromal powder particles are displayed in Figure 1. The L-PBF Scancromal particles are mainly spherical, with some elongated particles and few satellites. The presence of satellites onto the biggest particles is due to particle collision with very fine particles during atomisation. At higher magnification, some needle-like features are visible onto the surface of some particles that tend to increase the surface roughness.



a) b) c)

Figure 1 – SEM investigations at different magnifications for L-PBF Scancromal powders in the as-received state.

Micrographs of cross-sections of L-PBF Scancromal particles are presented in Figure 2. Only a few particles exhibit internal porosity as shown in Figure 2-b and 2-c. The pores can have a spherical shape, originating from gas bubbles incorporated during atomisation (Figure 2-b), or may originate when a liquid droplet collides with an already solid particle, creating a shell with an incomplete contact zone with the inner particle (Figure 2-c).



a) b) c)

Figure 2 – L-PBF Scancromal cross-sectional SEM micrographs in BSE mode and at different magnifications.

Figure 3 shows polished powder particles from Scancromal and Lean-Scancromal powders

exhibiting their internal microstructure in BSE mode. The internal microstructure varies considerably from one particle to another.

A significant difference can be observed at higher magnification between Scancromal and Lean-Scancromal powders (Figure 3d-f). Some white snow-like flakes are present in the Scancromal particles whereas blocky precipitates are more randomly distributed in both alloy systems. The snow-like flakes are presumably related to large primary Cr-rich and Mo-rich dendrites.

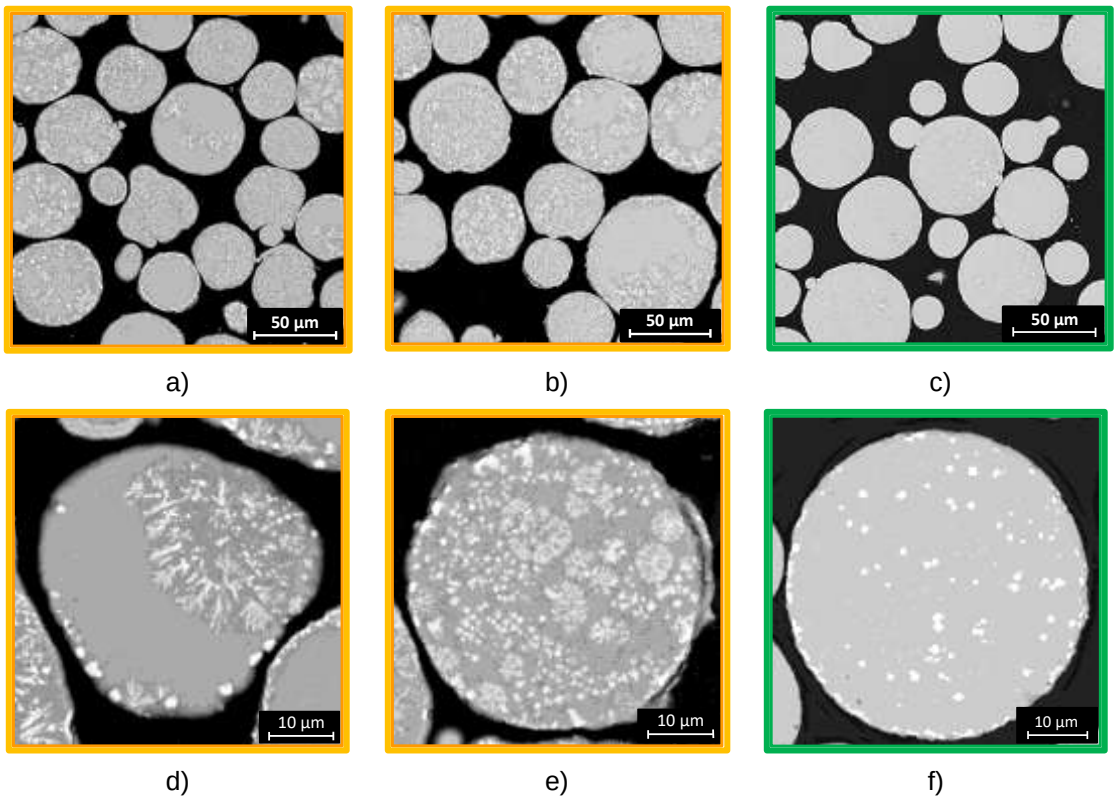
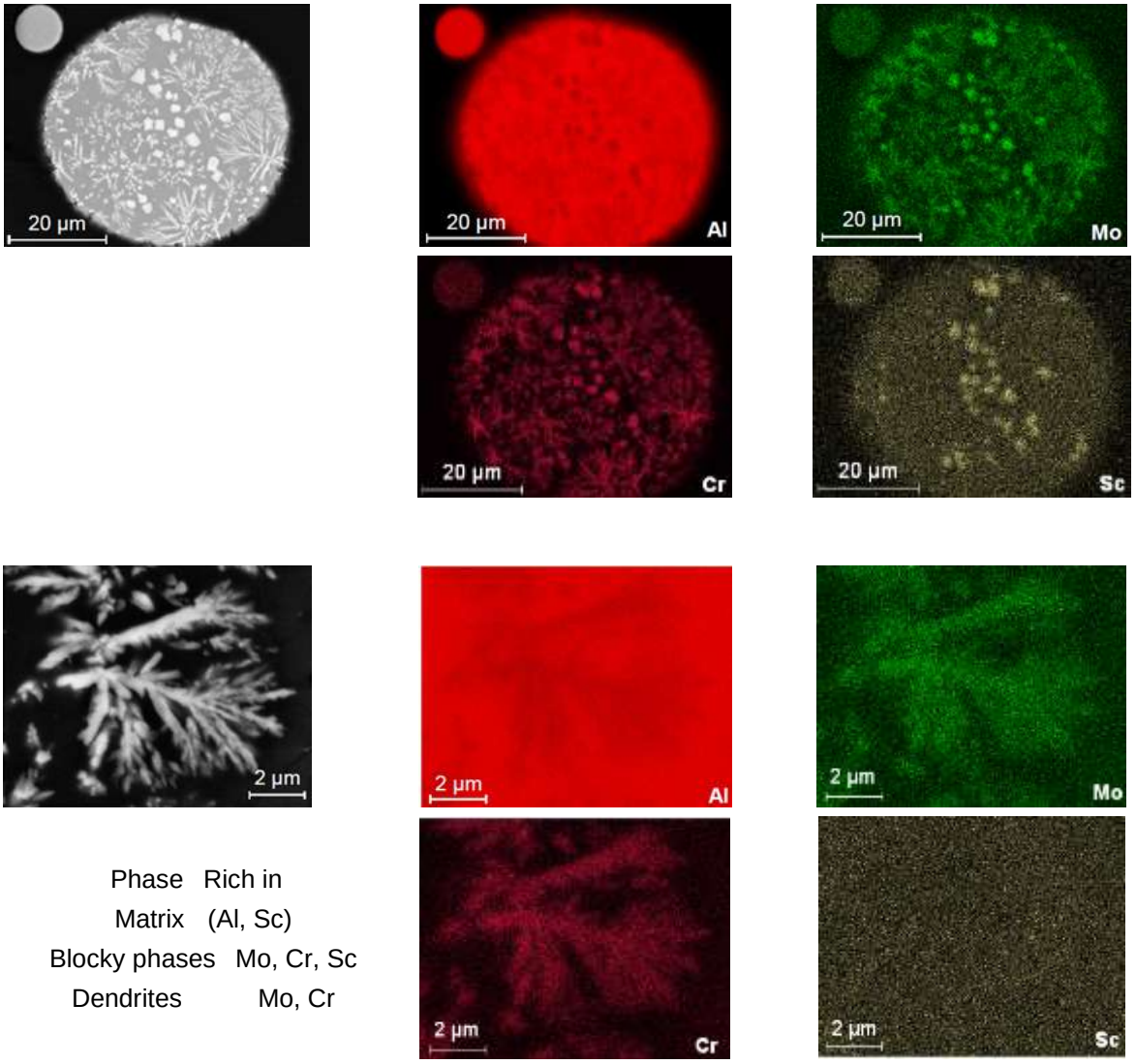


Figure 3 – SEM investigations using BSE mode for L-PBF polished powders: a), b), d (and e) Scancromal powders (orange frame), c) and f) Lean-Scancromal powders (green frame).

SEM/EDX mappings for L-PBF Scancromal powder are illustrated in Figure 4, showing the presence of Mo within the blocky phases and dendritic features. It should be noted that the Scancromal alloy contains a relatively high Mo content (approximately 1.3 wt.%).



Phase	Rich in
Matrix	(Al, Sc)
Blocky phases	Mo, Cr, Sc
Dendrites	Mo, Cr

Figure 4 – SEM/EDX mappings for a L-PBF Scancromal particle. Full cross-section and detailed analysis around a dendrite.

EDX analyses were performed on polished Scancromal and Lean-Scancromal powder particles, focusing on both the matrix and the precipitates (See Figure 5 and Table 7). The matrix exhibits relatively low Mo and Cr contents. The most significant observation is the presence of Mg in the Lean-Scancromal matrix, which is consistent with the alloy design, as Mg is not present in the Scancromal composition. Figure 5 also reveals the presence of Cr-, Mo-, Sc-rich precipitates in Scancromal powder, whereas Lean-Scancromal contains Cr- and Mg-rich precipitates.

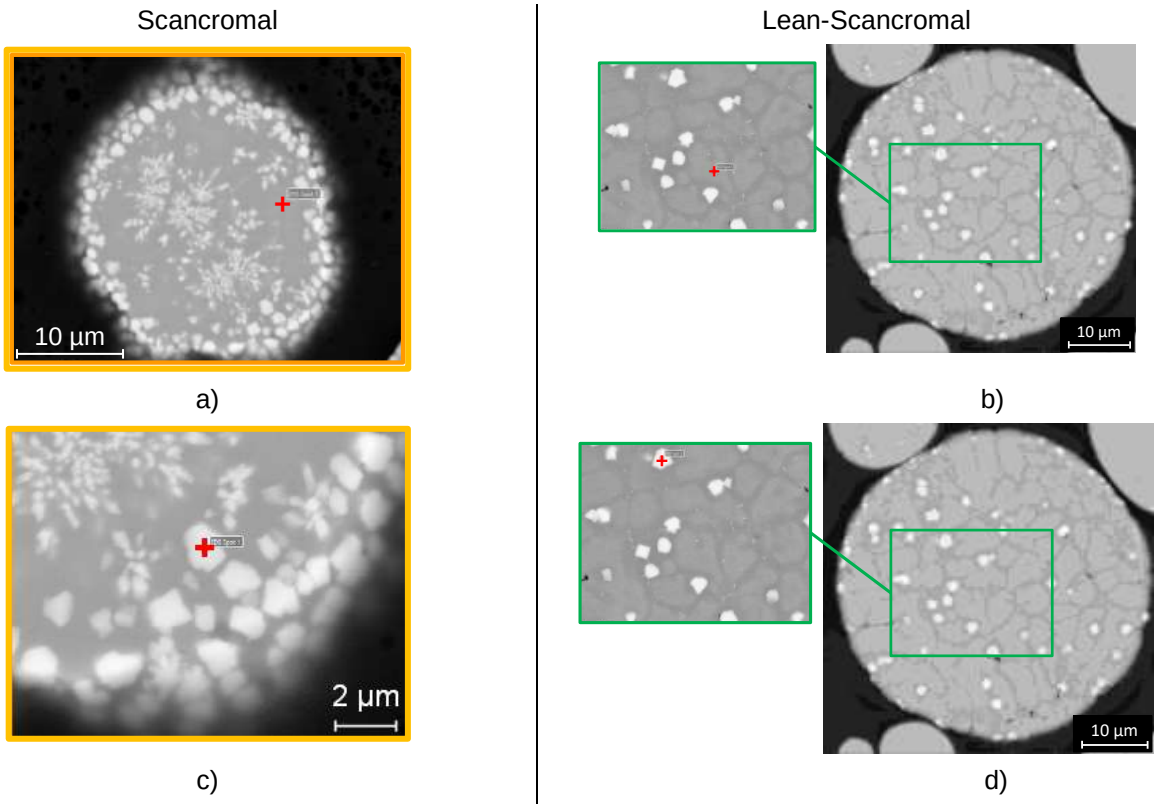


Figure 5 – EDX analysis location of the matrix (a and b) and precipitates (c and d) for L-PBF polished powders: Scancromal (a and c, orange frame), Lean-Scancromal (b and d, green frame).

Table 7 Local compositions in weight percentage (see Figure 5 – EDX analysis location of the matrix (a and b) and precipitates (c and d) for L-PBF polished powders: Scancromal (a and c, orange frame), Lean-Scancromal (b and d, green frame).

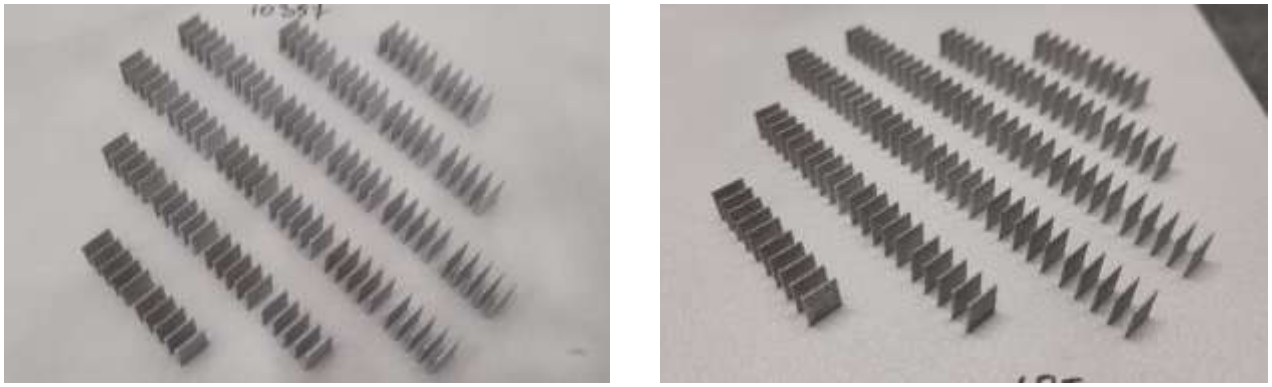
Wt.%	**Scancromal**		**Lean-Scancromal**	
Element	matrix	blocky precipitate	matrix	blocky precipitate
Al	98.0	89.2	95.6	91.5
Sc	0.6	1.5	0.6	0.9
Cr	1.2	5.1	1.7	2.5
Mo		3.5	0.5	0.8
Mg			1.4	3.1
Others (O, P, Si…)	0.2	0.7	0.2 (Si)	0.6 (Si) + 0.6

Overall, the SEM and EDX analyses confirmed the high sphericity and low defect content of both powders, together with compositional segregation features characteristic of the atomisation process. These results indicate that both alloy systems possess suitable morphological and microstructural characteristics for subsequent L-PBF processing and parameter optimisation studies.

3.2 Process optimisation

3.2.1 Thin walls

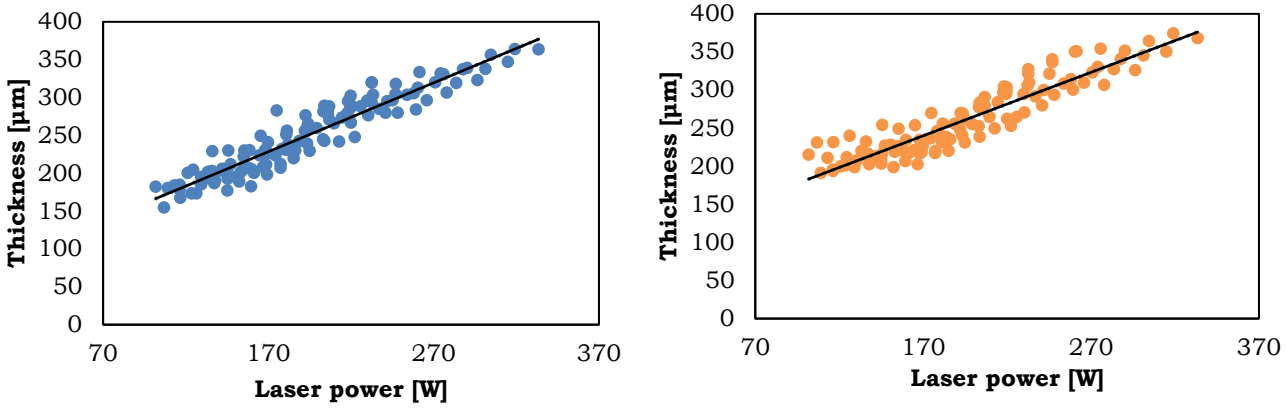
For the process optimisation step, first, thin walls were produced. A wide range of parameters were evaluation and a total of 120 thin walls were made per material, as can be seen in Figure 6.



a) b)

Figure 6 – L-PBF thin walls produced with a) Scancromal and b) Lean-Scancromal powders.

In order to analyse the thin walls and select the parameters, the cross-sections of the walls were taken. The microscopy images were analysed and the thickness, roughness, and porosity were measured. The results are plotted in Figure 7. When looking at the thickness, both powders show a similar linear correlation with the laser power and the thickness; the higher the laser power, the higher the thickness. Regarding the roughness, Lean-Scancromal samples show slightly higher values for the whole parameter range. A slight decrease in roughness is observed when increasing the laser power. Lastly, the porosity trend is slightly different between the two powders. Slightly lower porosities are observed for the low laser power values in Scancromal, whereas Lean-Scancromal shows a big scatter for all laser powers. In general, a higher porosity percentage is found for Lean-Scancromal walls. This methodology allows the selection of contour parameters depending on the final application. For example, when a low porosity is needed near to the surface of the parts, it is recommended to use a low power for the Scancromal powder.



a) b)

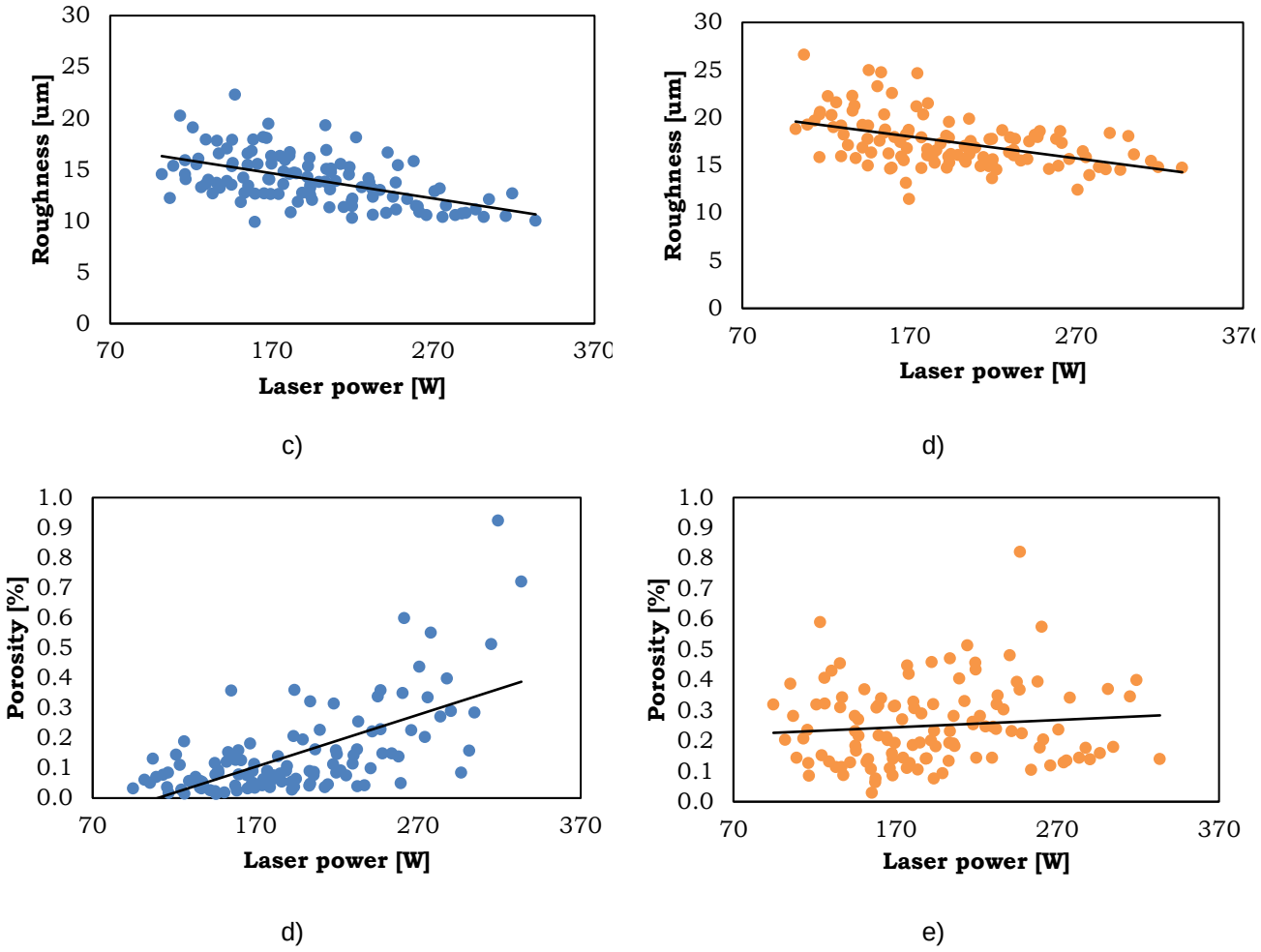
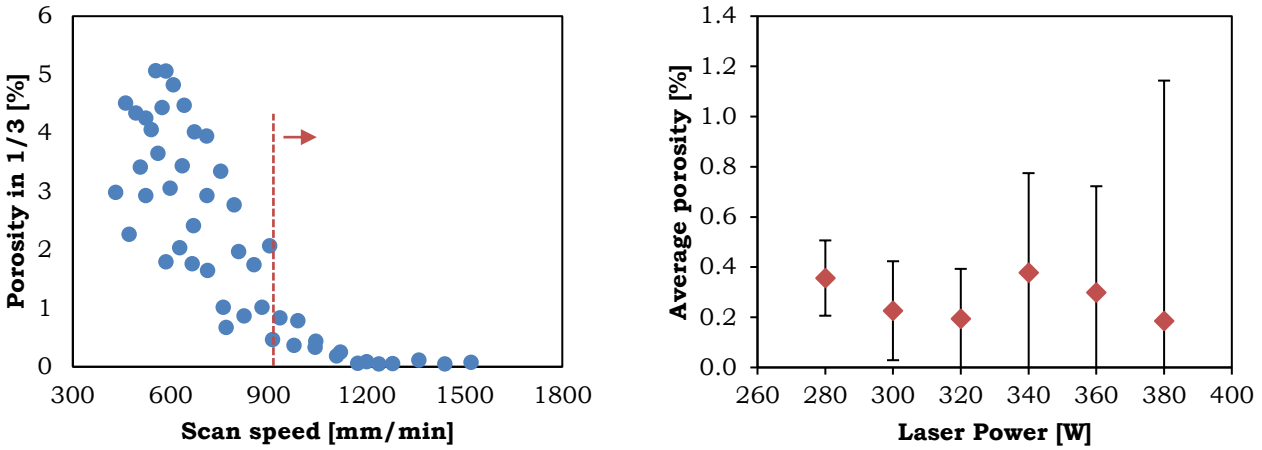


Figure 7 – Thickness (a-b), roughness (c-d) and porosity (e-f) of Scancromal (a,c,e) and Lean-Scancromal (b,d,f) thin walls as a function of the laser power.

3.2.2 Variable hatch blocks

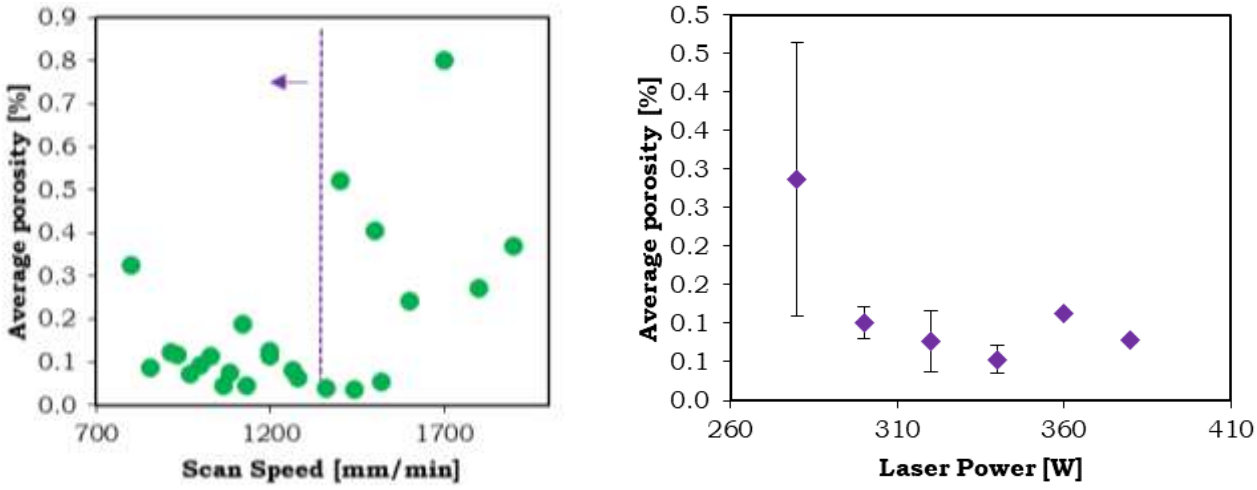
In order to evaluate the results of the variable hatch blocks, the blocks were cut in half, perpendicular to the change of hatch distance, the cross-sections were examined in porosity. Additionally, the porosity of each block can be examined as a function of the hatch distance. In Figure 8, the selection steps followed for Scancromal blocks are shown. In Figure 8-a, the average porosity over a third of the blocks is shown as a function of the scan speed, where each dot represents one blocks. A strong dependency of the scan speed on the porosity is observed. Particularly, above 900 mm/min, the porosity drops to values below 1%. In Figure 8-b, the blocks with speeds below 900 mm/min were removed and the porosity was plotted as a function of the laser power. In this figure, the average porosity was plotted. It can be observed that at higher laser powers, the average porosity increases as well as the spread over the porosity values. The minimum was found for 320 W blocks which were then selected for the next step.



a) b)

Figure 8 – Porosity plots for Scancromal variable hatch blocks as a function of a) scan speed and b) laser power for speeds higher than 900 mm/min.

After Scancromal blocks, Lean-Scancromal blocks were processed. Since it was found that the porosity is largely dependent on the speed, the parameter range was limited and readjusted to avoid low scan speeds. The porosity evaluation of the Lean-Scancromal blocks is shown in Figure 9. First, the porosity was plotted as a function of the scan speed, shown in Figure 9-a. The porosity increases with increasing the scan speed, in contrast to the observations in Scancromal. Above 1400 mm/min, a high porosity and spread is observed. When removing the high speed blocks and plotting them as a function of the laser power (Figure 9-b), the lowest deviation and porosity value is obtained for 340 W.

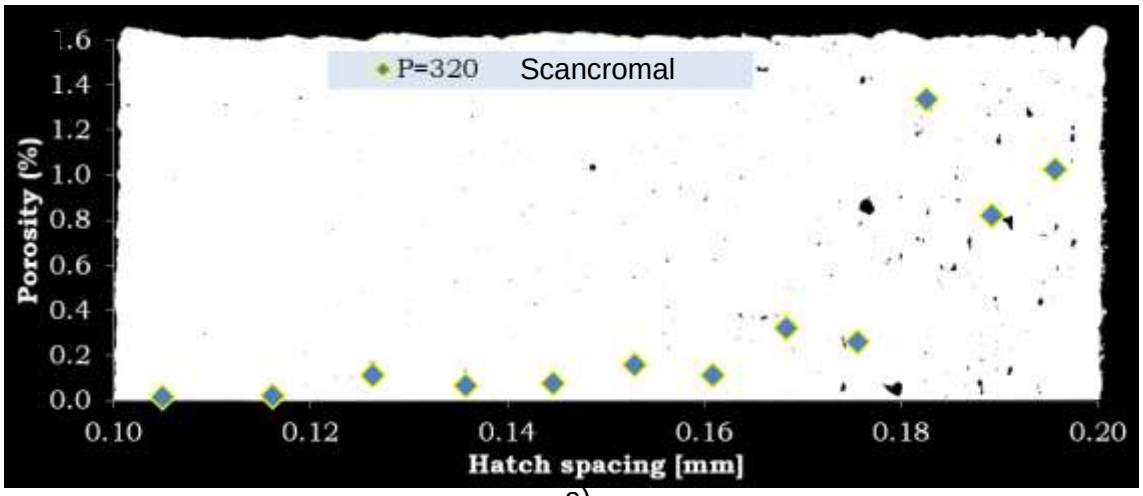


a) b)

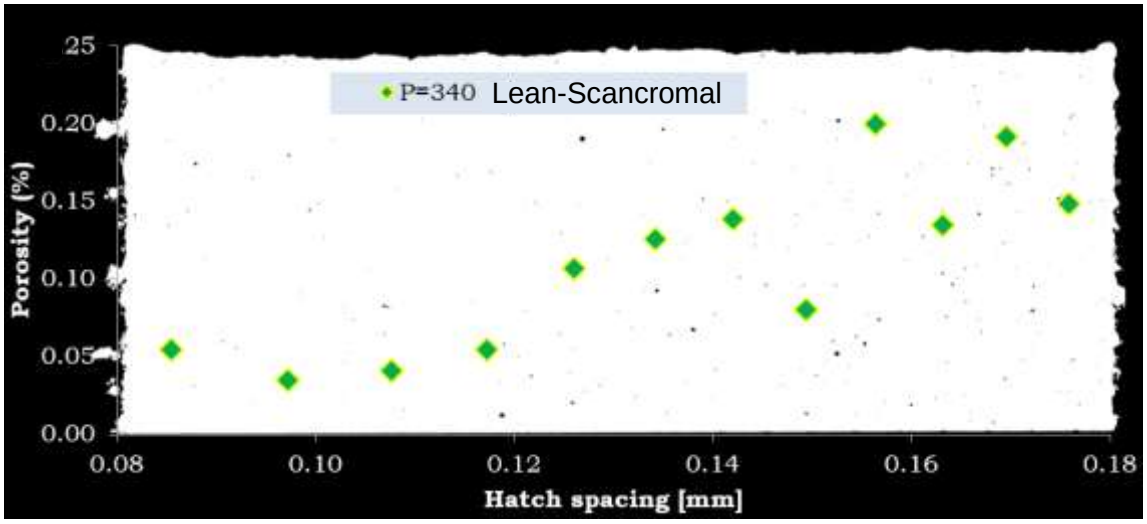
Figure 9 – Variable hatch block porosity for Lean-Scancromal powder. a) porosity as a function of the scan speed and b) as a function of the laser power.

After selecting the laser power and scan speed (or P/v), the hatch distance was selected. In Figure 10, the porosity graphs as a function of the hatch spacing are shown, also showing the polished cross-sections for both materials. For Scancromal, the lowest porosities are obtained for the smallest hatch distance, 0.1 mm. After obtaining these results, a lower hatch distance range was evaluated for Lean-Scancromal (from 0.08 to 0.18 mm). Overall, a lower porosity percentage is shown for Lean-

Scancromal samples. Nevertheless, the hatch distances around 0.1 mm resulted in the lowest porosity and therefore 0.1 mm was selected.



a)



b)

Figure 10 – Polished cross-sections of a) Scancromal and b) Lean-Scancromal showing the porosity percentage as a function of the hatch spacing along the variable hatch block.

4. Conclusions

Two novel aluminium alloy powders, Scancromal and Lean-Scancromal, were successfully characterised and processed by laser powder bed fusion (L-PBF).

Powder characterisation by sieve analysis, SEM observations, laser diffraction and flowability measurements demonstrated that both alloy systems exhibited particle size distributions and powder morphologies suitable for L-PBF processing. Lean-Scancromal showed a narrower PSD distribution, whereas Scancromal exhibited slightly better flowability behaviour.

Microstructural investigations by SEM, BSE and EDX revealed predominantly spherical particles with limited satellite formation and low internal defect content. In addition, compositional segregation features associated with the atomisation process were identified, including Cr-, Mo- and Sc-rich precipitates in Scancromal powders and Mg-containing phases in Lean-Scancromal powders.

Process parameter optimisation based on thin walls and variable hatch blocks allowed the

identification of suitable laser parameter combinations for both alloy systems. The obtained results demonstrated the importance of balancing porosity and surface quality during parameter selection.

Overall, the investigated alloy systems showed promising L-PBF processability and are expected to contribute to the wider industrial implementation of high-strength aluminium alloys for aerospace additive manufacturing applications.

5. Contact Author Email Address

maria.montero@nlr.nl

6. Copyright Statement

The authors confirm that they, and/or their company or organization, hold copyright on all of the original material included in this paper. The authors also confirm that they have obtained permission, from the copyright holder of any third party material included in this paper, to publish it as part of their paper. The authors confirm that they give permission, or have obtained permission from the copyright holder of this paper, for the publication and distribution of this paper as part of the ICAS proceedings or as individual off-prints from the proceedings.

7. References

[1] E. Louvis, P. Fox, and C. J. Sutcliffe, 'Selective laser melting of aluminium components', *J. Mater. Process. Technol.*, vol. 211, no. 2, pp. 275–284, 2011, doi: https://doi.org/10.1016/j.jmatprotec.2010.09.019.

[2] N. T. Aboulkhair, C. Tuck, I. Ashcroft, I. Maskery, and N. M. Everitt, 'On the Precipitation Hardening of Selective Laser Melted AlSi10Mg', *Metall. Mater. Trans. A*, vol. 46, no. 8, pp. 3337–3341, Aug. 2015, doi: 10.1007/s11661-015-2980-7.

[3] N. Kaufmann, M. Imran, T. M. Wischeropp, C. Emmelmann, S. Siddique, and F. Walther, 'Influence of Process Parameters on the Quality of Aluminium Alloy EN AW 7075 Using Selective Laser Melting (SLM)', *Phys. Procedia*, vol. 83, pp. 918–926, 2016, doi: 10.1016/j.phpro.2016.08.096.

[4] J. H. Martin, B. D. Yahata, J. M. Hundley, J. A. Mayer, T. A. Schaedler, and T. M. Pollock, '3D printing of high-strength aluminium alloys', *Nature*, vol. 549, no. 7672, pp. 365–369, Sep. 2017, doi: 10.1038/nature23894.

[5] M. L. Montero-Sistiaga *et al.*, 'Changing the alloy composition of Al7075 for better processability by selective laser melting', *J. Mater. Process. Technol.*, vol. 238, pp. 437–445, Dec. 2016, doi: 10.1016/j.jmatprotec.2016.08.003.

[6] 'Octomec expands capabilities with aluminium AM using LENS DED', Metal AM, May 06, 2020. [Online]. Available: https://www.metal-am.com/optomec-expands-capabilities-with-aluminium-am-using-lens-ded/

[7] K. Schmidtke, F. Palm, A. Hawkins, and C. Emmelmann, 'Process and Mechanical Properties: Applicability of a Scandium modified Al-alloy for Laser Additive Manufacturing', *Phys. Procedia*, vol. 12, pp. 369–374, 2011, doi: 10.1016/j.phpro.2011.03.047.

[8] L. Xi *et al.*, 'Effect of TiB2 particles on microstructure and crystallographic texture of Al-12Si fabricated by selective laser melting', *J. Alloys Compd.*, vol. 786, pp. 551–556, 2019, doi: https://doi.org/10.1016/j.jallcom.2019.01.327.

[9] D. Gu *et al.*, 'Selective Laser Melting Additive Manufacturing of TiC/AlSi10Mg Bulk-form Nanocomposites with Tailored Microstructures and Properties', *8th Int. Conf. Laser Assist. Net Shape Eng. LANE 2014*, vol. 56, pp. 108–116, Jan. 2014, doi: 10.1016/j.phpro.2014.08.153.

[10] 'Aluminium A20X Datha sheet', 3T-AM. Accessed: Jul. 10, 2020. [Online]. Available:

https://www.3t-am.com/sites/threeT/files/Aluminium%20A20X_Datasheet.pdf

[11] 'Scalmalloy (R)', APWorks. Accessed: Jul. 10, 2020. [Online]. Available: https://apworks.de/en/scalmalloy/

8. Acknowledgements

This research was carried out within the framework of GARTEUR, Action Group 36.